Journal of Magnetic Resonance 198 (2009) 24–30

Contents lists available at ScienceDirect

Journal of Magnetic Resonance

journal homepage: www.elsevier.com/locate/jmr

^{35}Cl profiling using centric scan SPRITE with variable flip angle excitation

Konstantin V. Romanenko [a], P.F. de J. Cano-Barrita [b], Bruce J. Balcom [a,*]

[a] MRI Centre, Department of Physics, University of New Brunswick, P.O. Box 4400, Fredericton, NB, Canada E3B 5A3
[b] CIIDIR IPN Unidad Oaxaca, Hornos No. 1003, Sta. Cruz Xoxocotlan, Oaxaca, Mexico

ARTICLE INFO

Article history:
Received 29 October 2008
Revised 4 December 2008
Available online 19 January 2009

Keywords:
SPRITE
Centric scan
^{35}Cl MRI
Relaxation time
Non-proton
Portland cement

ABSTRACT

An efficient MRI technique for quantitative density profiling of samples with fast spin-lattice relaxation (T_1 < 5 ms) is introduced. The pulse scheme is based on the 1D centric scan SPRITE technique. Strong excitation of the sample at the k-space origin improves the sensitivity with respect to the original centric scan SPRITE technique. Radio frequency pulse durations are defined so as to provide uniform excitation of the sample at every k-space point. For a particular k-space point the pulse duration is required to be less than the inverse sample bandwidth. Simulations permit one to examine distortions from ideal profile geometry due to flip angle and spin-lattice relaxation effects. The proposed technique is especially suitable for the observation of low sensitivity samples, in particular, low-γ nuclei like ^{35}Cl. In some cases, this strategy permits one to reduce the number of scans, i.e. the experiment time, by a factor of 100, depending on hardware, sample length and tolerable resolution loss. The designed pulse scheme is tested on cylindrical agar gel and type 1 Portland cement paste phantoms prepared to provide ^{1}H and ^{35}Cl signals, respectively.

1. Introduction

Single point imaging (SPI) is now widely accepted as a powerful quantitative technique for imaging objects with short spin-lattice, T_1, and spin–spin, T_2, relaxation times [1–4]. SPI and its later modification SPRITE (Single Point Ramped Imaging with T_1 Enhancement) [5] are pure phase encoding techniques. The gradient is increased stepwise, and a single point of the free induction decay (FID) is acquired at each step. Radio frequency (RF) excitation and signal acquisition are separated by a constant phase encoding delay, t_p. Magnetic field inhomogeneity and chemical shift artifacts, common for frequency encode imaging, are largely non-existent in SPI imaging [6].

The original SPRITE sequence introduces T_1 contrast through saturation of magnetization from ensembles with T_1 longer than the SPRITE repetition time, *TR* [5]. A centric scan modification of the SPRITE technique is built of two parts separated by a recovery interval $5 \times T_1$, Fig. 1. Each part acquires independently the k-space for positive and negative *k*-values starting from the k-space origin [7]. This results in an improved signal-to-noise ratio (SNR). The T_1/TR ratio is the critical factor affecting the image quality. The repetition time *TR* is commonly less than T_1 and this results in partial saturation of longitudinal magnetization, and a complex dependence of the measured signal on T_1/TR that leads to image blurring. Various sequences with magnetization preparation are designed to control image contrast and perform relaxation time mapping [7].

MRI of low γ nuclei is not straightforward due to reduced signal-to-noise ratio and various hardware limitations. Our interest is focused primarily on objects with short T_2^* and low γ. In many cases of practical importance, such samples also feature short T_1. In order to reduce the encoding time t_p at a fixed field of view (FOV), usable gradients should reach very high magnitudes ($\sim$100 G $\times$ cm^{-1}). This causes an additional limitation related to inhomogeneous excitation of the object by an RF pulse. Single point imaging (SPI) methods are based on non-selective RF pulses. To this point literature studies have employed RF pulses of constant duration at every k-space point. This RF pulse duration is governed by the available RF transmitter power and the product of the gyromagnetic ratio of an observed nucleus, γ, maximum gradient strength, G_{max}, and sample length, L_S. For commonly used imaging hardware this pulse duration corresponds to a small flip angle, $\alpha < 10°$. Thus, the requirement of homogeneous excitation severely restricts the sensitivity of the method, especially if low sensitivity nuclei, like ^{35}Cl, are observed. Limited ^{35}Cl MRI studies are available in the literature. To the best of our knowledge, the only two studies employ earlier generations of SPRITE methods [8,9].

The signal-to-noise ratio of a measured profile would significantly increase if larger flip angles were applied to the first k-space points assuming sample excitation to be homogeneous. Application of variable pulse durations over k-space is equivalent to apodization of k-space data with a weighting function. Fourier transform analysis says that any decaying function will cause profile blurring.

* Corresponding author. Fax: +1 506 453 4581.
E-mail address: bjb@unb.ca (B.J. Balcom).

1090-7807/$ - see front matter © 2009 Elsevier Inc. All rights reserved.
doi:10.1016/j.jmr.2009.01.007

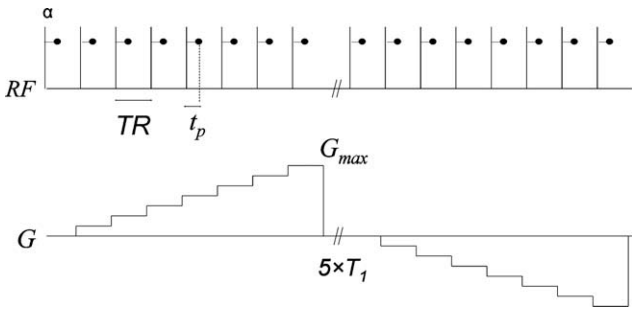

Fig. 1. Timing diagram of the centric scan SPRITE method. The phase-encoding gradient G is ramped along the selected direction. A single complex point is acquired at each gradient step a time t_p after the application of an RF pulse, with flip angle α.

High duty cycle RF pulses applied in SPRITE can cause extensive sample heating in samples with high ionic strength. The use of variable flip angles for *in vivo* SPRITE applications was introduced by Kaffanke et al. to minimize the specific absorption rate (SAR) [10]. In their work the RF pulse power was modulated maintaining the pulse duration, and therefore the bandwidth, constant. Based on this method SAR can be reduced by about 25% compared with standard SPRITE. This can be essential to prevent human tissues from heating by the radiated RF energy. Minimization of SAR is not only important for live systems but also for materials that change their structure on heating.

In the present paper the advantages and limitations of the centric scan SPRITE sequence with variable RF pulse duration (referred to as SPRITE-vpd) are outlined.

2. Theory

A rectangular profile Π_o of n points is Fourier transformed to model the k-space data, S_o, subject to apodization with an appropriate RF pulse duration envelope and T_1 weighting. The k-values are defined for $j = 0$ to $n/2-1$ as

$$k_{\pm j} = \pm j \times K_{\max} \times (n/2-1)^{-1}, \tag{1}$$

where

$$K_{\max} = \gamma \times G_{\max} \times t_p \times (2\pi)^{-1}. \tag{2}$$

The RF pulse duration corresponding to a $\pi/2$ flip angle at a given transmitter power is defined as $P_{\pi/2}$. The duration of the very first RF pulse in the sequence ($k_0 = 0$) is set to a value $P_\alpha \leqslant P_{\pi/2}$ corresponding to a flip angle α. Any pulse $P_\alpha > P_{\pi/2}$ will have an unwanted effect on the spin system.

For $j > 0$ the duration of the RF pulse exciting a sample bandwidth W_j can be defined as

$$P_j = W_j^{-1}, \tag{3}$$

where

$$W_j = (2\pi)^{-1} \times \gamma \times G_{\max} \times L_S \times (n/2-1)^{-1} \times j. \tag{4}$$

Depending on the sample bandwidth, $\gamma \times G_{\max} \times L_S$, some initial values W_j^{-1} can be larger than $P_{\pi/2}$ and P_α. In our model we assume that P_j is a decreasing function of j and all pulse durations are not larger than P_α. Thus, if $W_j^{-1} \geqslant P_\alpha$, the corresponding pulse duration P_j is set to P_α.

P_α defines the resulting MRI profile amplitude, and the signal-to-noise ratio. The pulse durations (Eq. 3) are chosen to excite the whole sample uniformly. Given the first pulse P_α, any pulse P_{Xj} longer than P_j defined by Eqs. (3 and 4) will not excite the sample uniformly at the k-space point k_j. Any set of pulses P_{Xj} so that $P_{Xj} < P_j$ will result in lower profile amplitude and/or stronger blurring with respect to that obtained with P_j, Eqs. (3 and 4). The later is a basic property of the Fourier transformation. A function that decays faster has a broader spectrum.

The maximum bandwidth is defined as

$$W_{\max} = W_{n/2-1} = (2\pi)^{-1} \times \gamma \times G_{\max} \times L_S. \tag{5}$$

The longest pulse homogeneously exciting the object at every k-space point that would be used in the original centric scan SPRITE scheme is defined as

$$P_\omega = P_{n/2-1} = W_{\max}^{-1} = (2\pi) \times (\gamma \times G_{\max} \times L_S)^{-1}. \tag{6}$$

Given that equilibrium Z magnetization, Mz_0, is 1, the longitudional magnetization, Mz_j, formed at time TR after the $(j-1)_{\text{th}}$ RF pulse, P_{j-1}, can be defined as

$$Mz_j = 1 - (1 - Mz_{j-1} \times \cos(P_{j-1} \times P_{\pi/2}^{-1} \times \pi/2)) \times \exp(-TR/T_1), \tag{7}$$

where j takes values from 0 to $n/2-1$; TR is the time interval between RF pulses. Assuming that $P_j \ll T_2^*$ the resulting transverse magnetization, i.e. the signal measured at k-space point k_j is given by

$$S(k_j) = S_o(k_j) \times \exp(-t_p/T_2^*) \times Mz_j \times \sin(P_j \times P_{\pi/2}^{-1} \times \pi/2), \tag{8}$$

The apodization function, $f(j)$, that accounts for the effects of RF saturation, variable RF pulse duration and transverse magnetization decay during the encoding time, t_p, is defined as:

$$f(j) = \exp(-t_p/T_2^*) \times Mz_j \times \sin(P_j \times P_{\pi/2}^{-1} \times \pi/2), \tag{9}$$

where one can assign

$$f_0(j) = Mz_j \times \sin(P_j \times P_{\pi/2}^{-1} \times \pi/2), \tag{9a}$$

An eventual simulated profile, $\prod$, is determined by the inverse Fourier transformation of $S(k_j)$.

The SPRITE-vpd profile amplitude is increased with respect to a centric scan SPRITE profile by a factor:

$$q = \sin(\alpha) \times \{\sin(\omega)\}^{-1}, \tag{10}$$

$$q = \sin(P_\alpha \times P_{\pi/2}^{-1} \times \pi/2) \times \{\sin(P_\omega \times P_{\pi/2}^{-1} \times \pi/2)\}^{-1}, \tag{10a}$$

The profile can be defined as a convolution of a real density distribution, the rectangular profile $\prod_o$ in our case, with the point spread function (PSF), F_{PSF}:

$$\prod = \prod_0 \otimes F_{\text{PSF}} \tag{11}$$

The latter, F_{PSF}, is obtained by inverse Fourier transformation of f.

3. Results and discussion

3.1. Simulations

The strategy for determination of the RF pulse duration at each k-space point described above provides maximum profile amplitude and homogeneous sample excitation at a given blurring level. The purpose of the present simulations is to demonstrate how P_α, $W_{\max}$, and T_1/TR ratio affect the profile of a rectangular object. The profile amplitude, i.e. the signal-to-noise ratio, and blurring both increase with P_α. Thus, obtaining optimal flip angles, α, at the k-space origin is crucial for efficient and quantitatively reliable profiling.

K-space was modeled with 64 points to conform to usual experiment. The reasonable ranges of parameters impacting the profile edge blurring, P_α, $W_{\max}$, and T_1/TR ratio, were considered for

simulation of the SPRITE-vpd experiment. A range of bandwidths, W_{max}, between 10 kHz and 1 MHz covers most available imaging gradients. The T_1/TR ratios considered were 0.01 and 2. The former T_1/TR value models the situation when the profile blurring due to RF saturation is negligible. The later T_1/TR refers a practical situation when some RF saturation is present. The flip angles at the k-space origin, α, were $\pi/2$, $\pi/3$, $\pi/6$, and $P_\omega \times (P_{\pi/2})^{-1} \times \pi/2$, where P_ω is defined by (Eq. 6).

The RF pulse durations vs. j are calculated for several sample bandwidths, W_{max}, given that $\alpha = \pi/2$, Fig. 2. It is remarkable that for a sufficiently narrow bandwidth, W_{max}, a $P_{\pi/2}$ pulse of 50 μs can be applied uniformly along k-space. Increasing W_{max} requires the range of RF pulse variation along the k-space to increase.

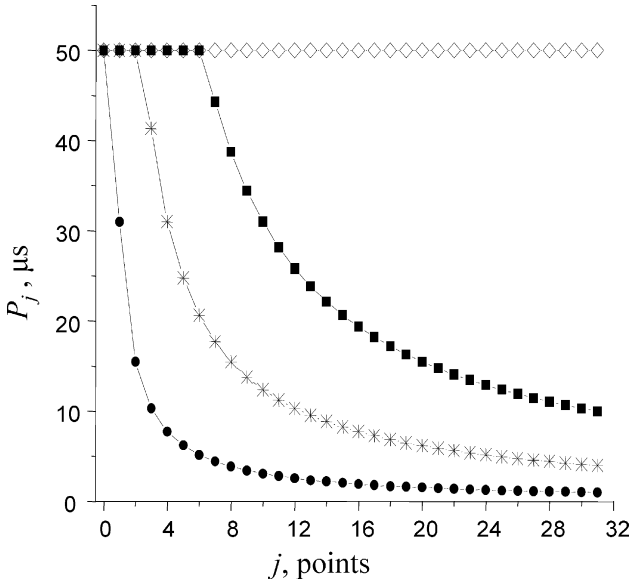

Fig. 2. Radio frequency pulse durations, P_j, versus k-space coordinate number, j, calculated for a SPRITE-vpd pulse sequence according to Eqs. (3 and 4). As the sample bandwidth increases, the sharper the RF pulse envelope becomes. The simulation parameters were $P_\alpha = P_{\pi/2} = 50$ μs; $W_{max} = 10$ kHz (◇), 100 kHz (■), 250 kHz (*), 1000 kHz (●).

SPRITE-vpd becomes less reliable in terms of blurring artifacts when the maximum allowable RF power is low, so that the $P_{\pi/2}$ pulse is unreasonably long, i.e. $\geqslant$100 μs. Our calculations were performed for $P_{\pi/2} = 50$ μs. For a longer $P_{\pi/2}$ the blurring would be greater.

The effect of P_α on resolution of the method is clearly seen in the case of fast spin-lattice relaxation, $T_1/TR = 0.01$, Fig. 3. Examples of the normalized PSF calculated for a set of W_{max} noted above, and $\alpha = \pi/2$ and $\pi/6$ are displayed in Fig. 3(a and b), respectively. Higher W_{max} values cause wider PSFs. However, that effect can be compensated by selection of a starting pulse duration P_α lower than $P_{\pi/2}$.

RF saturation of Mz is an additional source of resolution loss in SPRITE-vpd. The appodization functions, $f_0(j)$, determined for a set of W_{max}, and T_1/TR of 0.01 and 2, are shown in Fig. 4(a and b), respectively. The first RF pulses strongly reduce the magnetization in the case of longer T_1, Fig. 4b.

The SPRITE-vpd profiles simulated with T_1/TR of 0.01 and 2 are shown in Figs. 5 and 6, respectively. In the case of T_1/TR equal 2 and α of $\pi/2$ the profiles are extremely broad, Fig. 6(a–d), that is manifested as broad side tails or elevated baseline. Apparently reducing the flip angle, α, eliminates this broadening. The profiles simulated for T_1/TR of 0.01 and 2 are very similar for $\alpha \leqslant \pi/6$, Fig. 5(a′′–d′′) and Fig. 6 (a′′–d′′), respectively.

The signal improvement factor, q (Eq. 10a), is greater for higher W_{max} and α. For any fixed W_{max} the maximum q is reached at α of $\pi/2$. However, one should be aware of corresponding edge blur, that is not acceptable for $T_1 \geqslant TR$ and large flip angles at k-space origin. In the range of W_{max} noted above, $T_1/TR \leqslant 2$ and $\alpha \leqslant \pi/6$ the blurring seems to be acceptable for regular profiling. These approaches have been tested experimentally on cylindrical agar gel and cement paste phantoms.

3.2. Experiments

The gradient strength, encoding time, RF transmitter power, and probe ring-down time are the most important hardware-related parameters in SPRITE-vpd. In SPRITE-vpd effective phase encoding may occur during the longer RF pulses. The $P_{\pi/2}$ pulses typically used in these studies were within a range between 50 and 100 μs that is comparable to typical phase encoding times, t_p, Table 1. Large variation of the RF pulse duration within the SPRITE-vpd sequence causes

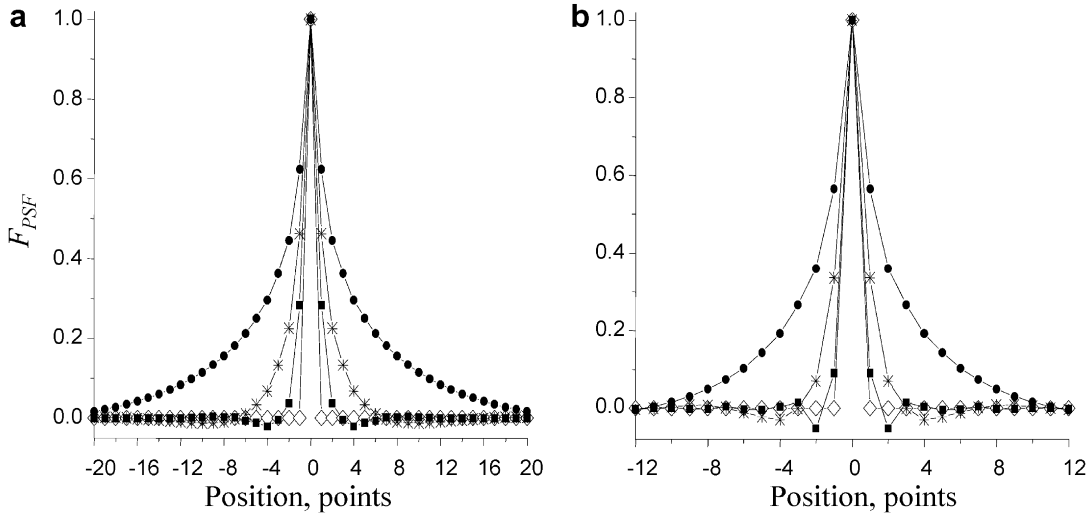

Fig. 3. Point spread functions, F_{PSF}, obtained by inverse Fourier transformation of normalized apodization functions f_0, Eq. (9a). Profile broadening described by its point spread function strongly depends on the flip angle by the first RF pulse, α. The simulation parameters were $P_{\pi/2} = 50$ μs; (a) $\alpha = \pi/2$, $T_1/TR = 0.01$; (b) $\alpha = \pi/6$, $T_1/TR = 0.01$; $W_{max} = 10$ kHz (◇), 100 kHz (■), 250 kHz (*), 1000 kHz (●).

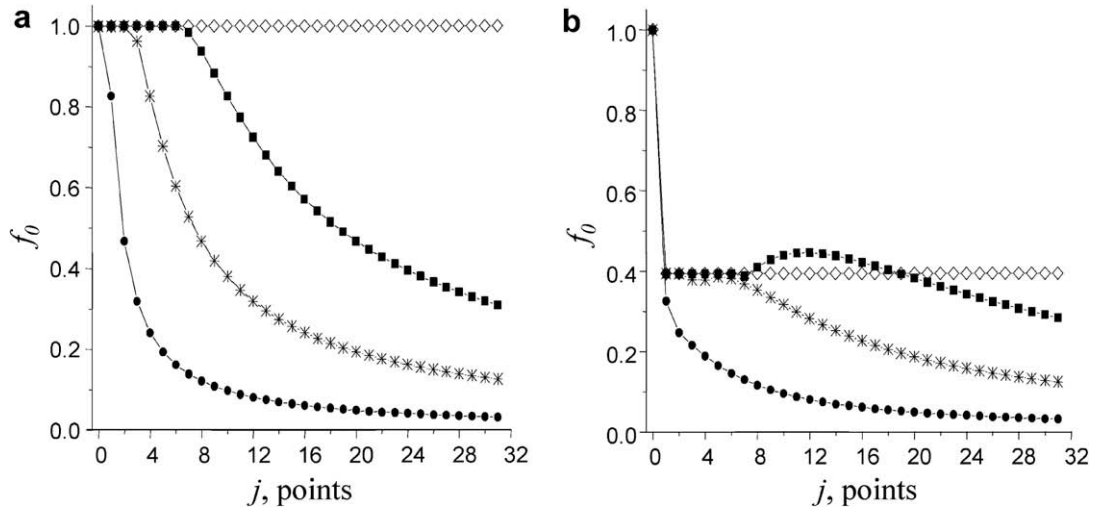

Fig. 4. The normalized apodization functions, f_0, given by Eq. (9a) for one half of the k-space. The simulation parameters were $P_\alpha = P_{\pi/2} = 50$ μs; (a) $T_1/TR = 0.01$; (b) $T_1/TR = 2$; $W_{max} = 10$ (◇), 100 (■), 250 (*), 1000 kHz (●). The larger T_1/TR ratio results in a remarkable amplitude decrease after the first RF pulse that is a typical cause of severe profile blurring.

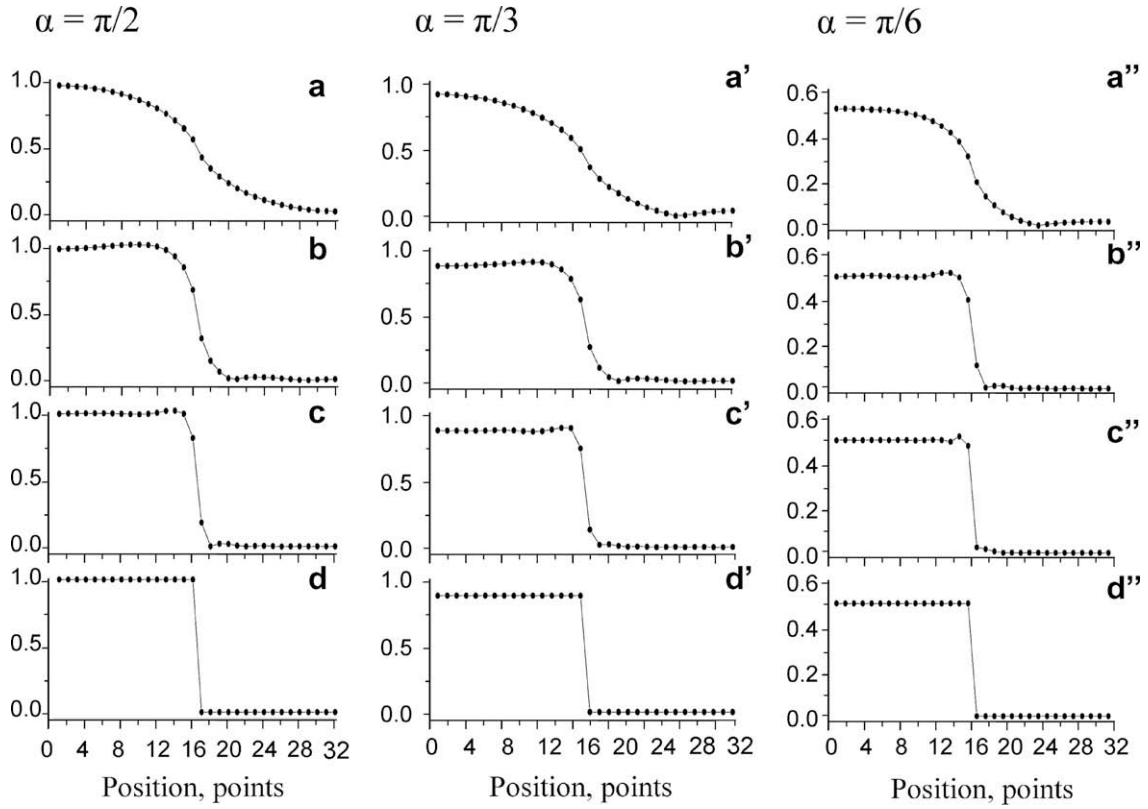

Fig. 5. Simulated profiles (32 positive points), ∏, obtained by Fourier transformation of $S(k_j)$ given by Eq. (8). The simulation parameters were $T_1/TR = 0.01$; $P_{\pi/2} = 50$ μs; $\alpha = \pi/2$, $\pi/3$, $\pi/6$; (a, a′, a″) $W_{max} = 1000$ kHz; (b, b′, b″) $W_{max} = 250$ kHz; (c, c′, c″) $W_{max} = 100$ kHz; (d, d′, d″) $W_{max} = 10$ kHz. The RF saturation effects are negligible since the T_1/TR ratio is very low. The predicted blurring is due to variation of the RF pulse duration only.

non-linear phase encoding and, therefore, unacceptable profile distortion. The problem is essentially eliminated if the encoding time is considered to commence at the center of each RF pulse excitation. In most cases the RF pulse durations were much smaller than T_2^*.

The ^{1}H profiles measured for two cylindrical agar gels phantoms, A_1 and A_2, are shown in Fig. 7A$_1$ (a–f) and A$_2$ (a′–f′), respectively. Experimental parameters are listed in Table 1. The maximum bandwidth, W_{max}, was set at 155 ± 5 kHz. The P_α values varied in the range from $P_{\pi/2}$ to P_ω. The edge blurring increased with P_α. Minor profile distortions could result from the residual non-linear phase encoding effect described above. It can not be totally eliminated for an RF pulse of a finite width. This effect decreases with decreasing P_α.

For the phantom A_1 a T_1/TR ratio of 0.4 was sufficiently low to eliminate the effects of RF saturation, Fig. 7(A_1). Apparently the blurring was finely controlled by P_α. In the case of $\alpha = \pi/2$ the SNR increased by the factor of 6 with respect to that of original centric scan SPRITE, Fig. 7(a and f). It is very close to a factor q of

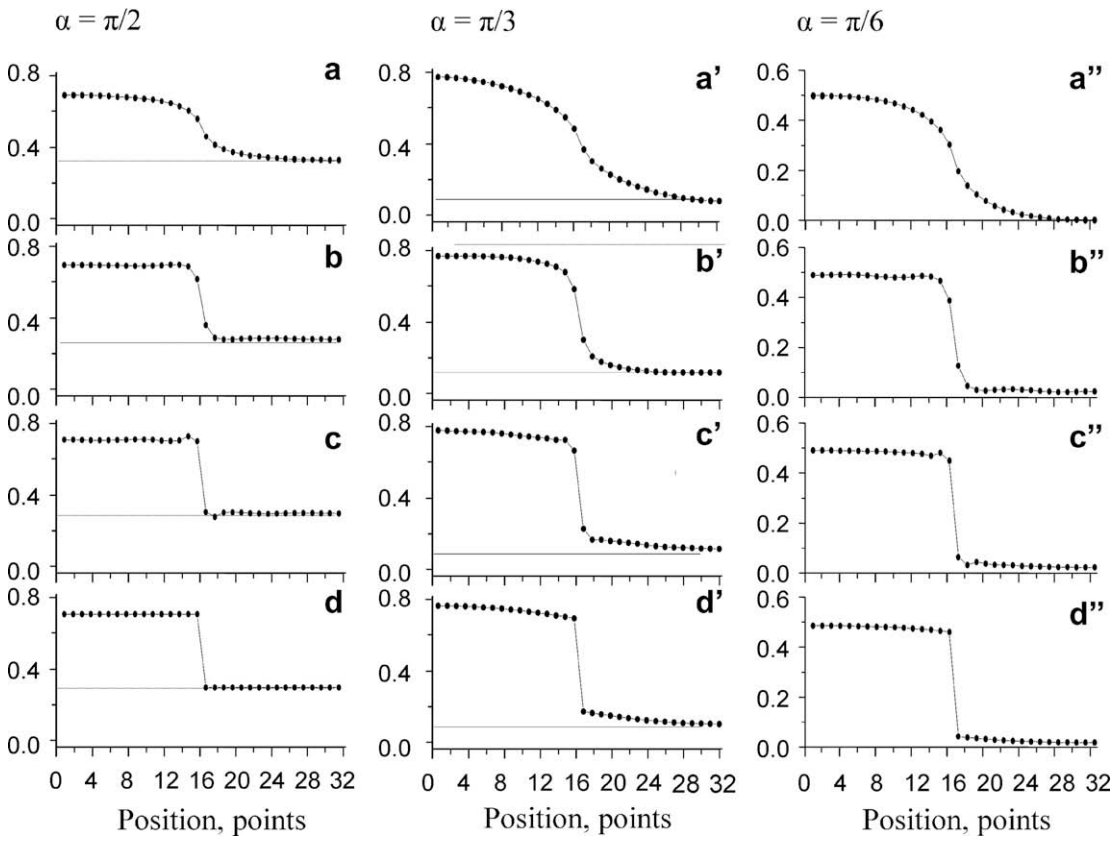

Fig. 6. Simulated profiles (positive 32 points), $\prod$, obtained by Fourier transformation of $S(k_j)$ given by Eq. (8). The simulation parameters were $T_1/TR = 2$; $P_{\pi/2} = 50$ μs; $\alpha = \pi/2$, $\pi/3$, $\pi/6$; (a, a′, a″) $W_{max} = 1000$ kHz; (b, b′, b″) $W_{max} = 250$ kHz; (c, c′, c″) $W_{max} = 100$ kHz; (d, d′, d″) $W_{max} = 10$ kHz. The RF saturation effects for $\alpha = \pi/2$ and $\pi/3$ are manifested as extremely broad side tails.

Table 1
L_S is the sample length; T_1 and T_2^* are the longitudinal and transverse relaxation time constants, respectively; W_{max} is the maximum sample bandwidth; P_ω is the largest pulse duration homogeneously exciting the object at every k-space point.

Samples	L_s (cm)	T_1 (ms)	T_2^* (ms)	W_{max} (kHz)	P_ω (μs)
A_1	3.9	0.8	0.35	155	6.5
A_2	4	4.1	1.2		
B_1	5.5	2	0.4	138	7.3

5.36 predicted by (Eq. 10a). Given $T_1/TR \leqslant 0.4$, $W_{max} < 160$ kHz and $P_{\pi/2} < 60$ μs one can use α as large as $\pi/2$ without risk of severe blurring. The T_1/TR ratio of 2 (A_2) causes unacceptable distortions for $\alpha > \pi/4$, Fig. 7(a′–c′).

The ^{35}Cl profiles obtained with SPRITE-vpd and original centric scan SPRITE pulse schemes are displayed in Fig. 8(a–c), respectively. Using SPRITE-vpd with α of $\pi/3$ (a) and $\pi/6$ (b) resulted in a dramatic increase in SNR with respect to the original centric scan SPRITE experiment. A profile edge blurring of 2–4 points was observed, Fig. 8(a and b).

The SPRITE experiment with a large constant RF pulse $P_\alpha \gg P_\omega$ may result in tolerable profile distortions as well as SPRITE-vpd. A particular disadvantage, in addition to non-uniform sample excitation, is the higher range of RF heating. This is especially important when the sample contains brine. The more charged ions in the sample, the more energy is deposited as heat. Our particular interest in ^{35}Cl relates to salt water invasion of porous materials, specifically the chlorine nucleus, since it is associated with corrosion processes. Our ^{35}Cl measurements were performed on cement paste samples with NaCl concentrations of 2.8 M. Seawater NaCl concentration is 0.5 M. The SPRITE-vpd scheme developed allows acquiring more signal averages without a risk of the object being dried out or unreasonably overheated. In our experiments with variable pulse duration the cement paste sample temperature remained at ambient temperature level, ~25 °C. The sample temperature increased to as much as 60 °C when a constant excitation flip angle of $\pi/6$ was applied.

4. Conclusion

The variable pulse duration centric scan SPRITE technique is well suited for 1D imaging of a wide variety of short T_1 systems. Using the inverse sample bandwidth for each gradient value as a strategy for determination of the SPRITE pulse durations provides maximum profile amplitude and homogeneous sample excitation at a given blurring level. The profile blurring is defined by the choice of RF power and duration of the very first pulse in the SPRITE sequence. This technique is designed to improve the signal-to-noise ratio in MRI measurements of extremely low sensitivity systems. The increase in sensitivity with respect to the original centric scan SPRITE is achieved through the use of larger magnetization flip angles at the k-space origin.

5. Experimental

Aqueous solutions of $GdCl_3$ (0.04–0.25 M) and agar powder (5 wt.%) were used to prepare agar gel phantoms 10 mm in diameter and approximately 40 mm long with required spin-lattice relaxation time constants, Table 1.

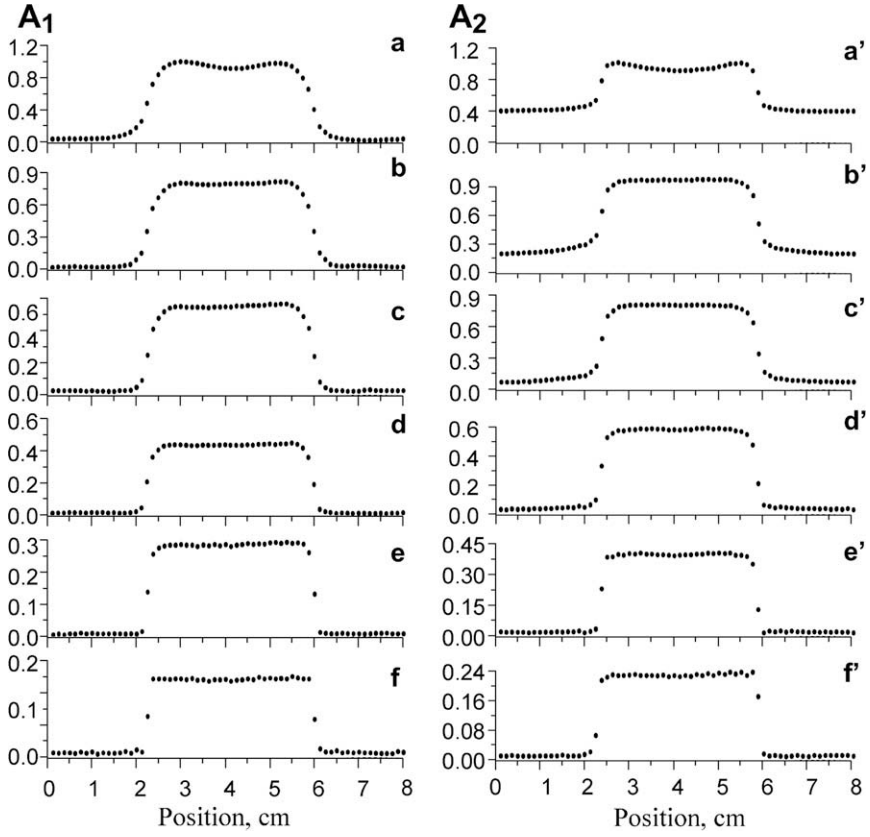

Fig. 7. The ^{1}H profiles of the agar gel phantoms A_1 (left column, short T_1) and A_2 (right column, long T_1) presented as a function of α: (a, a′) $\alpha = \pi/2$; (b, b′) $\alpha = \pi/3$; (c, c′) $\alpha = \pi/4$; (d, d′) $\alpha = \pi/6$; (e, e′) $\alpha = \pi/9$; (f, f′) Original centric scan SPRITE, $w = \pi/17$. $L_S = 4$ cm, $G_{max} = 9.1$ G × cm^{-1}, FOV = 8 cm, $NS = 4$. No baseline correction was applied to the raw k-space data.

Type 1 portland cement was used to prepare cylindrical cement paste phantoms 40 mm in diameter and 55 mm long. An appropriate volume of 2.8 M NaCl solution was thoroughly mixed with an amount of cement required to produce a cement paste with a water-to-cement ratio of 0.5. The cement paste cast in cylindrical glass containers of 41 mm in diameter was moist cured for 3 days at ambient temperature of 23 °C. The phantoms were cut from the initial cylindrical pieces so as to make sharp edges and, thus, achieve a rectangular profile. The phantoms were then covered with marine epoxy resin to prevent drying.

The samples, from 4 to 6 cm long, fit into the region of homogeneous B_1 of the RF coil and the region of linear gradient. The ^{1}H profiles were measured on a MARAN spectrometer (Resonance Instrument Ltd., Oxford, United Kingdom) equipped with a 7T wide-bore, horizontal superconducting magnet 7T/60/AS (Magnex Scientific Ltd., Oxford, United Kingdom). A standard gradient set SGRAD156/100/S (Magnex Scientific Ltd., Oxford, United Kingdom) provided a maximum gradient strength of 40 G/cm. A home-made 62 mm inner diameter probe was used with an RF power amplifier 7T1000S (Communication Power Corp., New York, USA). The applied gradient strength, G_{max}, was 9.1 G × cm^{-1}. The $P_{\pi/2}$ pulse was 54 μs at 0.5 kW power. The encoding and repetition times, t_p and TR, were 0.1 and 2 ms, respectively. The ^{1}H profiles were acquired with 4 signal averages.

The ^{35}Cl profiles were measured using a Tecmag (Houston, TX) Apollo console equipped with a Nalorac (Martinez, CA) 2.4 T 32 cm i.d. horizontal bore superconducting magnet. A water cooled 75 mm i.d. gradient set driven by Techron (Elkhart, IN) 8710 amplifiers provided a gradient strength up to 100 G × cm^{-1}. The ^{35}Cl RF probe with a 32 rung quadrature birdcage coil (Morris Instruments, Ottawa) was driven by a 2 kW AMT (Brea, CA) 3445 RF amplifier.

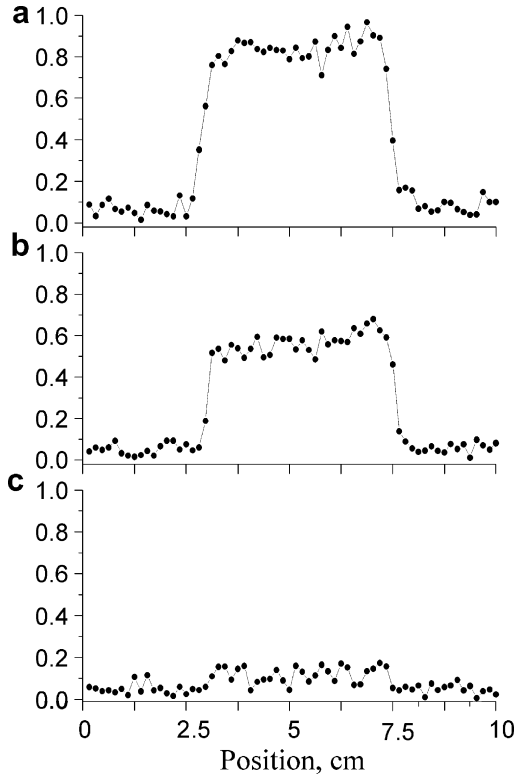

Fig. 8. The ^{35}Cl profiles of the cement paste phantom measured for different α: (a) $\alpha = \pi/2$; SNR ≈ 8.5 (b) $\alpha = \pi/3$; SNR ≈ 6 (c) original centric scan SPRITE, $\alpha = w = \pi/26$; SNR ≈ 1. $L_S = 5.5$ cm, $G_{max} = $ G × cm^{-1}, FOV = 10 cm, $NS = 32{,}000$ (2 h experiment time).

The applied gradient strength, G_{max}, was 60 G × cm^{-1}. The $P_{\pi/2}$ pulse was 95 μs at 0.65 kW power. The encoding and repetition times, t_p and *TR*, were 0.124 and 2 ms, respectively. The ^{35}Cl profiles were acquired with 32,000 signal averages.

The phantoms designations and the most important experimental parameters related to these samples are listed in Table 1. All measurements were carried out at ambient temperature. Numeric analysis was performed with Matlab 7.0 software.

Acknowledgments

The UNB MRI Centre is supported by an NSERC Major Resources Support Award. BJB acknowledges NSERC for Discovery and Equipment Grants and the Canada Chairs program for a Research Chair in MRI of Materials. P.F. de J. Cano acknowledges the support from the Instituto Politecnico Nacional de Mexico for the sabbatical year 2007–2008, and CONACYT from Mexico for a sabbatical scholarship.

References

[1] B.J. Balcom, SPRITE imaging of short relaxation time nuclei, in: P. Blümler, B. Blümich, R. Botto, E. Fukushima (Eds.), Spatially Resolved Magnetic Resonance, Wiley-VCH, Toronto, 1998, pp. 75–86.

[2] C.B. Kennedy, B.J. Balcom, I.V. Mastikhin, Three-dimensional magnetic resonance imaging of rigid polymeric materials using single-point ramped imaging with T_1 enhancement (SPRITE), Can. J. Chem. 76 (1998) 1753–1765.

[3] S.D. Beyea, B.J. Balcom, P.J. Prado, A.R. Cross, C.B. Kennedy, R.L. Armstrong, T.W. Bremner, Relaxation time mapping of short T_2^* nuclei with single-point imaging methods, J. Magn. Reson. 135 (1998) 156–164.

[4] P.J. Prado, B.J. Balcom, I.V. Mastikhin, A.R. Cross, R.L. Armstrong, A. Logan, Magnetic resonance imaging of gases: a single-point ramped imaging with T_1 enhancement (SPRITE) study, J. Magn. Reson. 137 (1999) 324–332.

[5] B.J. Balcom, R.P. MacGregor, S.D. Beyea, D.P. Green, R.L. Armstrong, T.W. Bremner, Single-point ramped imaging with T_1 enhancement (SPRITE), J. Magn. Reson. A 123 (1996) 131–134.

[6] S. Gravina, D.G. Cory, Sensitivity and resolution of constant-time imaging, J. Magn. Reson. A 104 (1994) 53–61.

[7] I.V. Mastikhin, B.J. Balcom, P.J. Prado, C.B. Kennedy, SPRITE MRI with prepared magnetization and centric k-space sampling, J. Magn. Reson. 136 (1999) 159–168.

[8] F.de J. Cano, T.W. Bremner, R.P. McGregor, B.J. Balcom, Magnetic resonance imaging of ^{1}H, ^{23}Na, and ^{35}Cl penetration in Portland cement mortar, Cement Concrete Res. 32 (2002) 1067.

[9] F. de J. Cano-Barrita, B.J. Balcom, T.W. Bremner, Non-destructive determination of chloride and sodium distribution in Portland cement mortar, in: International Conference on Durability of High Performance Concrete, Essen, Germany, September 21–24, (2004) 351.

[10] J.B. Kaffanke, S. Romanzetti, T. Dierkes, B. Balcom, N.J. Shah, Turbo RF-SPRITE: methods to reduce acquisition time and SAR for *in vivo* applications, Proc. Intl. Soc. Magn. Reson. Med. 13 (2005) 2399.